SIMULATION OF SEMICONDUCTOR DEVICES AND PROCESSES Vol. 4
Edited by W. Fichtner, D. Aemmer - Zurich (Switzerland) September 12-14, 1991 - Hartung-Gorre

Oxygen Precipitation in CZ-Silicon During Multi-Step Annealing Cycles

Martin Schrems, Matthias Budil, Gerhard Hobler and Hans Pötzl*
Institut für Allgemeine Elektrotechnik und Elektronik, TU Vienna, A-1040 Vienna, Austria
* also: *Ludwig Boltzmann-Institut für Festkörperphysik, A-1060 Vienna, Austria*

Jürgen Hage
Wacker-Chemitronic GmbH, D-8263 Burghausen, Germany

Abstract

Our recently developed model for oxygen precipitation is applied to multi-step thermal anneals including a CMOS-type cycle. The model is in good agreement with experimental results. Alternatives for a redesign of the CMOS-process are investigated. Precipitates forming during crystal growth in the temperature range from $1000°C$ to $700°C$ as well as during temperature ramping are shown to influence results significantly. We also present a generalized kinetic concept for modelling coupled diffusion-precipitation phenomena, which contains our previous precipitation model as special case.

Controlling the formation of SiO_2-type agglomerates of oxygen and silicon (oxygen precipitates) inside CZ-wafers during thermal anneals is important for obtaining a high yield in manufacturing VLSI/ULSI devices. Oxygen precipitation inside the bulk is utilized for the removal of harmful metal impurities from device active regions ("internal gettering"). Designing the gettering behaviour during complicated annealing cycles requires a detailed knowledge of size and number of the oxygen precipitates inside the wafer.

The purpose of this work is to calculate number and size of precipitates in the bulk of the wafer, during multi-step annealing cycles like those in CMOS technology. Most of the currently used computer models for precipitation phenomena cannot be used for this task. Simple "clustering models" developed for arsenic precipitation (e.g.[1]) use the unjustified assumption, that all precipitates have equal size which is constant with time. Models based on Ham's theory of diffusion [2],[3] assume a constant number of precipitates which is used as a free parameter. Monte Carlo models as reported by Hawkins [5] require considerable computational resources and to our knowledge have not been applied to multi-step thermal processes so far. Models based on Fokker-Planck equations provide an efficient means for calculating the concentration of precipitates as a function of precipitate size and time, which yields all necessary data (total concentration of precipitated oxygen, average concentration and size of oxygen precipitates) [6]. Nevertheless the Fokker-Planck equations, which are based on a Taylor series expansion of a corresponding set of rate equations, fail at describing the smallest precipitates containing only a few atoms [4]. Therefore we have recently developed a computer model [8] for oxygen precipitation, which allows an adequate description of all precipitate sizes at manageable computation times, by combining rate equations for small precipitate sizes with a Fokker-Planck equation for all larger ones. The kinetic model equations are a special case of a generalized kinetic concept, which allows the systematic derivation of kinetic equations for arbitrary coupled diffusion-precipitation phenomena. The kinetic concept is outlined in the following section.

1 Generalized kinetic models for coupled diffusion-precipitation phenomena

1.1 General set of precipitation equations

As the host medium a crystalline solid is assumed. We define a "precipitate" as any particle or compound of particles that differs in its composition from the ideal crystal lattice. This means e.g. in the case of oxygen in silicon, that even a single vacancy, a single silicon selfinterstitial, or a single oxygen atom is a precipitate just as well as an extended defect like a dislocation, a stacking-fault, or an oxygen-silicon agglomerate composed of millions of atoms. In the following this definition will allow a unified theoretical description of precipitate formation starting from single particles and leading to extended defects. The fundamental qualities of a precipitate are its "type" and the "position" of its center of mass with respect to a coordinate system fixed in the crystal lattice. The type σ of a precipitate is completely determined by the number of particles n_i of the species T_i (i=1,2...s) and by the position of the individual particles with respect to the center of mass.

$$\sigma \equiv (n, a_n) \equiv (n_1, n_2, n_3, ...n_s; a_n) \tag{1}$$

The integer number a_n accounts for all different geometric configurations, which cannot be transformed into each other by a change of the coordinate system. Its maximum possible value is called A_n. We assume that there is a volume d^3x (with the coordinates $\vec{x} = (x_1, x_2, x_3)$ of its center), in which the concentration of those precipitates, which can move in the lattice, is approximately constant with space. On the other hand d^3x shall be large compared to sizes of the mobile precipitates. The concentration of precipitates of type σ inside the volume d^3x can change with time either by precipitate motion (**"diffusion"**) into or out of d^3x or by a transition of its type from σ to μ or vice versa (**"precipitation"**)

$$\sigma \equiv (n; a_n) \rightarrow \mu \equiv (m; a_m) = (n + k; a_{n+k}) \tag{2}$$

with n and $m = n + k$ being abbreviations for the "composition" of the precipitates with the type σ or μ

$$n \equiv (n_1, ... n_i, ... n_s) \quad m \equiv (m_1, ... m_i, ... m_s) = n + k \equiv (n_1 + k_1, ... n_i + k_i, ... n_s + k_s) \tag{3}$$

Any changes k_i of the particle numbers n_i at the transition (3) must not result in negative particle numbers ($n_i + k_i \geq 0$). The variation with time (t) of the concentration $f_\sigma(\vec{x}, t)$ of the precipitates with type σ in d^3x is determined by the continuity equation

$$\frac{\partial f_\sigma(\vec{x}, t)}{\partial t} = -\nabla \vec{j}_\sigma + \sum_\mu (f_\mu w_{\mu\rightarrow\sigma} - f_\sigma w_{\sigma\rightarrow\mu}) + Q_\sigma \tag{4}$$

The first term $-\nabla \vec{j}_\sigma(\vec{x}, t)$ on the right hand side of equation (4) accounts for the increase of f_σ due to diffusion into the volume d^3x, while the second and the third term yield the number of precipitates σ generated or lost by transitions from or to other precipitate types. The transition rates from μ to σ and from σ to μ are denoted by $w_{\mu\rightarrow\sigma}(\vec{x}, t)$ and $w_{\sigma\rightarrow\mu}(\vec{x}, t)$. If σ and μ are equal $w_{\sigma\rightarrow\sigma} = 0$ is demanded. For the net number of transitions from σ to μ we introduce a "precipitation flux"

$$I_{\mu\rightarrow\sigma}(\vec{x}, t) = f_\mu w_{\mu\rightarrow\sigma} - f_\sigma w_{\sigma\rightarrow\mu} \tag{5}$$

which will be useful for simplifying the notation in the sections below. The sum $\sum_\mu$ in equation(4) as well as the sum $\sum_\sigma$ are short forms of

$$\sum_\mu = \sum_{m_1=0}^{N_1}\sum_{m_2=0}^{N_2}\cdots\sum_{m_s=0}^{N_s}\sum_{a_m=1}^{A_m} \qquad \sum_\sigma = \sum_{n_1=0}^{N_1}\sum_{n_2=0}^{N_2}\cdots\sum_{n_s=0}^{N_s}\sum_{a_n=1}^{A_n} \tag{6}$$

N_i $(1 \leq i \leq s)$ is the maximum number of particles of the species T_i that a precipitate can contain and A_m (A_n) denotes the maximum number of geometric configurations possible for a particle with composition m (n). The additional term $Q_\sigma(\vec{x},t)$ in equation (4) guarantees **"conservation of particles"** at the "pure" precipitation process

$$0 = \sum_\sigma n_i \cdot \left(\frac{\partial f_\sigma(\vec{x},t)}{\partial t}\right)_{prec} = \sum_\sigma n_i \cdot \left(\sum_\mu (f_\mu w_{\mu\to\sigma} - f_\sigma w_{\sigma\to\mu}) + Q_\sigma\right) \tag{7}$$

for each species T_i and $(i = 1,\ldots s)$. The conservation of particles holds only in case T_i is an impurity atom. If T_i is an interstitial matrix atom, or a vacancy the Frenkel pair generation/recombination mechanism has to be considered in Q_σ too. In physical terms Q_σ accounts for a change in f_σ if precipitates of the (mobile) type σ are consumed or generated during a transition of another precipitate from $\bar{\sigma}$ to $\bar{\mu}$.

Equations (4) and (7) describe the general case of coupled diffusion-precipitation phenomena. They serve as master equations for *systematically* deriving simplified kinetic equations. The simplification is always achieved by specifying the number s of the precipitating species, the permitted changes k_i of the particle number n_i at any transition of precipitate type and the types σ of those precipitates, which are mobile (diffuse) in the host crystal. We have derived a number of special cases in this way including e.g. a model with two precipitating species, that may be applied to the formation of precipitates of oxygen and carbon with changing stochiometric composition. For brevity we can only demonstrate the method for the case of one precipitating species in this paper.

1.2 One precipitating species, change of particle number ± 1

There shall be only one precipitating species $(s = 1)$, and we assume that there is only one geometric configuration for any precipitate composition n $(A_n = 1)$, which means that the numbers "a_n, a_m" in equations (1)– (7) can be omitted. The notation is simplified by setting $n = n_1$ and $N = N_1$. It is assumed, that the particle number $n = n_1$ can only change by $k_1 = \pm 1$ at any single transition, and that only single particles diffuse. Therefore the precipitate types σ and μ reduce to $\sigma = (n_1) = (n)$, $\mu = (m_1) = (n \pm 1)$. Additionally, $\vec{j}_{(n)} = \vec{0}$ and $Q_{(n)} = 0$ for $n \neq 1$ follows. This is due to the restriction, that only precipitates consisting of one particle can diffuse. Therefore the precipitates "(1)" are the only ones that can be generated or consumed at a transition of other precipitate types.

By introducing the above conditions into equations (4) and (7) and by using the definition of the precipitation flux (5) we obtain

$$\frac{\partial f_{(1)}(\vec{x},t)}{\partial t} = -\nabla\vec{j}_{(1)} - I_{(1)\to(2)} + Q_{(1)} \qquad (n=1) \tag{8}$$

$$\frac{\partial f_{(n)}(\vec{x},t)}{\partial t} = I_{(n-1)\to(n)} - I_{(n)\to(n+1)} \qquad (n = 2,3,\ldots N) \tag{9}$$

$$Q_{(1)} = -\sum_{n=2}^{N} I_{(n-1)\to(n)} \qquad I_{(n-1)\to(n)} = f_{(n-1)}w_{(n-1)\to(n)} - f_{(n)}w_{(n)\to(n-1)} \tag{10}$$

In deriving equation (8) it has to be considered, that no particles are generated or annihilated ($w_{(0)\to(1)} = w_{(1)\to(0)} = 0$). Additionally, we consider $I_{(N)\to(N+1)} = 0$ for $n = N$ in equation (10), since the maximum N of the number n of particles of the species T_1 cannot be exceeded ($w_{(N)\to(N+1)} = w_{(N+1)\to(N)} = 0$). This model has been proposed earlier [7] and will be the basis for describing the precipitation kinetics of oxygen in silicon later. Another potential application may be modelling the formation of precipitates of other dopants like Sb,... or metals.

1.3 Kinetic rate equations in combination with a Fokker-Planck equation

Usually both small precipitates consisting of a few atoms and very large precipitates with millions of atoms can form during thermal anneals. Even in the simple case of section 1.2 this leads to millions of coupled kinetic rate equations like equations (9), which cannot be solved at manageable computation times. Therefore the sets of kinetic rate equations (equations (4)) are usually expanded ("Kramers-Moyal expansion" [10]) into a Taylor series with respect to the changes k_i in the particle numbers n_i , which are assumed quasi-continous. Termination of the series after second order terms yields a single "Fokker-Planck" equation approximating the whole set of rate equations. In case of the equations (9) in section 1.2 the Kramers-Moyal expansion and some straightforward manipulations lead to the following Fokker-Planck equation:

$$\begin{aligned} \frac{\partial f(n;\vec{x},t)}{\partial t} &= -\frac{\partial I(n;\vec{x},t)}{\partial n} \\ I(n;\vec{x},t) &= -B\cdot\frac{\partial f}{\partial n} + A\cdot f \end{aligned} \tag{11}$$

with the coefficients A,B depending on the transition rates $w_{(n)\to(n-1)}$, $w_{(n)\to(n+1)}$

$$A(n;\vec{x},t) = -\frac{\partial B}{\partial n} + w_{(n)\to(n+1)} - w_{(n)\to(n-1)} \tag{12}$$

$$B(n;\vec{x},t) = \frac{1}{2}\cdot\left(w_{(n)\to(n+1)} + w_{(n)\to(n-1)}\right) \tag{13}$$

Similar to equation (9) $f(n;\vec{x},t)$ denotes the concentration of precipitates of type "(n)" (...containing n particles of the species T_1). Nevertheless we write $f(n;\vec{x},t)$ instead of $f_{(n)}(\vec{x},t)$ indicating that the domain for n has been extended to non-negative real values. The disadvantage of the Fokker-Planck equation is that it provides a bad approximation for the smallest precipitate sizes containing only a few atoms. Recently [7], [8] we have therefore suggested a combined system of rate equations for small precipitate sizes and a Fokker-Planck equation for all larger ones linked by appropriate boundary conditions. In case of one precipitating species and a permitted change of the particle number of ± 1 such a combined system consists of equations (8)–(9) for $n = 1$ up to a user specified index $n = n_0$ and the Fokker-Planck equation (11) for $n_0 + 1 \le n \le N$. The rate equation (9) for $n = n_0$ and the Fokker-Planck equation are linked by a boundary condition for the precipitation flux

$$I(n_0+1;\vec{x},t) = f_{(n_0)}w_{(n_0)\to(n_0+1)} - f(n_0+1;\vec{x},t)w_{(n_0+1)\to(n_0)} = I_{(n_0)\to(n_0+1)} \tag{14}$$

Finally, it has to be considered, that in the term $Q_{(1)}$ in equation (10) for $n \ge n_0 + 1$ the following substitutions have to be made

$$n \in \mathcal{N}_0 \to n \in \mathcal{R}_0^+ \qquad f_{(n)}(\vec{x},t) \to f(n;\vec{x},t) \qquad \sum_{n=n_0+1}^{n=N} \to \int_{n=n_0+1}^{n=N} \tag{15}$$

with $\mathcal{N}_0$ being the set of non-negative integers and $\mathcal{R}_0^+$ denoting the set of non-negative real numbers. (8)–(10) and (11)–(15) are the set of combined kinetic equations obtained earlier[7].

In order to apply the sets of kinetic equations derived from (4) and (7) to real physical systems, the diffusion fluxe(s) $\vec{j}_\sigma$ and transition rates $w_{\mu\to\sigma}, w_{\mu\to\sigma}$ have to be modelled. An expression for $\vec{j}_\sigma$ can be obtained by considering the jumps of mobile precipitates from one lattice site to another. Since it is known from literature [10] that transitions of precipitate sizes and jumps in a crystal lattice are a mathematically identical problem, it is clear that jumps in the crystal lattice are described by a term identical to the second term in equation (4). This time $\sigma = (y_1, y_2, y_3)$ and $\mu = (z_1, z_2, z_3)$ denote positions in the crystal lattice. The transition rates w are interpreted as jump rates to neighbouring positions. Performing a Kramers Moyal expansion leads to a Fokker-Planck equation now called diffusion equation, the coefficients of which depend on the jump rates. They are mathematically identical to the equations derived for precipitation. In this way modelling diffusion or precipitation is referred to modelling jump rates or transition rates. In the simple case of equal and constant jump rates, this leads to Fick's law of diffusion for j_σ. More refined models for jump rates have recently been used [9] to derive equations for diffusion under influence of mechanical stress.

2 Transition rates for oxygen precipitation in silicon

Oxygen precipitation in silicon is described by the combined set of kinetic equations (8)–(10) and (11)–(15). All coefficients in the equations are determined by the transition rates $w_{(n)\to(n+1)}$ (growth) and $w_{(n)\to(n-1)}$ (dissolution) of an oxygen precipitate containing n oxygen atoms, which are modelled by [8]

$$w_{(n)\to(n+1)} = h \cdot C_O^{if}, \qquad w_{(n)\to(n-1)} = h \cdot C_{O0}^{if} \tag{16}$$

Expressions for the concentration C_O^{if} of oxygen atoms at the interface between precipitate and matrix and for its equilibrium value C_{O0}^{if} can be derived as shown earlier [8]. For h the expression [8]

$$h = 4\pi r^2 \delta \cdot \nu \exp\left(\frac{-\Delta G_{(n)\to(n+1)}}{kT}\right), \qquad n = \frac{4\pi}{3v_O} \cdot r^3 \tag{17}$$

based on the assumption of spherical precipitates with radius r is used. r is related to the number of O-atoms as shown in the right equation in (17). $v_O \approx \frac{v_{SiO_2}}{2}$ is the volume per oxygen atom in the precipitate with stochiometric composition SiO_2. The thickness δ of the interface between precipitate and matrix in equation (17) is roughly equal to the distance between two Si atoms in the lattice (0.235 nm). ν denotes the frequency of attempts $\nu = D_O/\delta^2$ (D_O denotes the diffusion coefficient of oxygen) of the O-atoms to surmount the energy barrier

$$\Delta G_{n\to n+1} = \Delta G(n+1,t) - \Delta G(n,t) + \Delta G_{activation} \tag{18}$$

for incorporation into the precipitate. This requires an activation energy of $\Delta G_{activation} \approx 0.25eV$[11]. The Gibbs energy $\Delta G(n,t)$ of a precipitate containing n O-atoms, is modelled as the sum of volume energy ΔG_O and the interfacial energy ΔG^{if}

$$\Delta G_O = -n \cdot kT \ln\left(\frac{C_O}{C_O^{eq}}\right), \qquad \Delta G^{if} = 4\pi r^2 \cdot \alpha \cdot \left(1 + \left(\frac{\zeta}{n}\right)^{\frac{1}{3}}\right) \tag{19}$$

The average concentration of oxygen atoms C_O residing in interstitials sites in the silicon bulk is equal to the solution $f_{(1)}$ of equation (8) and C_O^{eq} is its value in case of thermodynamical equilibrium. The interfacial energy ΔG^{ij} contains a constant parameter $\alpha = 0.31 J/m^2$ [12] In difference to earlier work [8] a correction factor for the interfacial energy of small precipitates containing a free parameter ζ [13] is introduced. Point defects and precipitate stress are not considered, which is also contrary to earlier [8] work. This shall reduce the number of free parameters and allow the fitting of a large number of experimental data at manageable computations times.

3 Simulation Results

Only calculations for oxygen precipitation in the bulk of a silicon wafer are performed. Using ZOMBIE[14] we solve the combined kinetic equations (8)–(10) and (11)–(14) numerically, which yields the size distribution function $f(n,t) = f(n;t)$ as a function of the number of O-atoms in the precipitate and the annealing time. The dependence on the location $\vec{x}$ and the diffusion term $-\nabla \vec{j}_{(1)}$ are neglected, since the oxygen concentration in the bulk is approximately homogenous. Loss of bulk oxygen due to outdiffusion is a minor effect in all processes studied. Therefore it is only accounted for by error functions [7]. Experimentally observable quantities like the loss of interstitial oxygen $C_{O,loss}$ due to the formation of precipitates containing 2 or more O-atoms, the total concentration C_{OP} and the average precipitate radius $\bar{r}$ of those oxygen precipitates (OP) containing more than n_{res} particles, are evaluated according to

$$C_{O,loss} = \sum_{n=2}^{N} n \cdot f_{(n)}, \qquad C_{OP} = \sum_{n=n_{res}}^{N} f_{(n)}, \qquad \bar{r} = \frac{\sum_{n=n_{res}}^{N} r \cdot f_{(n)}}{\sum_{n=n_{res}}^{N} f_{(n)}} \tag{20}$$

and by considering equation (15). The number n_{res} is chosen as $0.5 \cdot 10^6$, which roughly corresponds to the resolution limit for precipitate sizes in the experimental determination of the concentration of precipitates by etch pit counting. As far as possible we have tried to take into account all thermal influences a sample has been exposed to. This includes temperature ramps before and after annealing as well as an estimate for the cooling time $t_{cooling}$ from 1400°C to 450°C during crystal growth. Simulation parameters have been determined using the optimization driver "PROFILE"[15] to match experimental [16] and calculated data of two-step anneals shown in Figs.1,2. The values obtained are $\zeta = 0.22$, the coefficients $C_{O0}^{eq} = 2.2 \cdot 10^{21} cm^{-3}$ and $E_O = 1.05 eV$ in the bulk equilibrium concentration of interstitial oxygen

$$C_O^{eq} = C_{O0}^{eq} \cdot \exp\left(\frac{-E_O}{kT}\right) \tag{21}$$

and an estimate of $t_{cooling} = 3h$ for the cooling time during crystal growth. (Only $\zeta = 0.22$ was universal in all simulations we performed). Comparing our model to the experimental results shown in Fig.3 and a number of other results not shown here the values of $C_{O0}^{eq} = 2.0 \cdot 10^{21} cm^{-3}$ and $E_O = 1.03 eV$ as observed experimentally by Craven [19] were found more accurate. Additionally a value of $t_{cooling} = 10h$ was used instead of $t_{cooling} = 3h$. The difference in parameter values is not surprising, since different samples may have different levels of point defect supersaturation and different levels of contamination with other impurities than oxygen (e.g. carbon), which cannot be considered in the model used here. Additionally the value of $t_{cooling}$ may be blurred by additional thermal pretreatments in the experiment which we did not know of.

In the following the model with parameters as in Fig.3 is used for estimating oxygen precipitation in a CMOS-type annealing cycle ("p3" in Tables 1ab). The simulation results for precipitated oxygen, the density and the average radius of the precipitates for the full cycle "p3" as well as its first ("p1") and second stage ("p2") are shown in Figs.4,5 and 6. The lines labeled with "p4" and "p5" will be discussed later. In Fig.4 experimental results for the loss of interstitial oxygen after "p1","p2" and the final CMOS-cycle "p3" are shown too. It can be seen that the experimental results are predicted quite well in most cases.

As mentioned before the formation of oxygen precipitates during cooling in CZ-crystal growth is accounted for by assuming an exponential decrease of temperature from 1400°C to 450°C in about 10h ("co1"). The subprocess 1 ("sp1") is intended for dissolving preexisting precipitates, especially those formed during crystal growth. Nevertheless it can be seen that the $1200°C$ steps contained in p1 (full lines in Figs.4,5,6) already lead to a significant amount of oxygen precipitation. For initial oxygen concentrations above $8.0 \cdot 10^{18} cm^{-3}$ almost all precipitates have already formed during the first stage "p1" of "p3"(Fig.5), while for the lower oxygen concentrations the majority of the precipitates have formed after the second stage "p2" due to the "sp3" (Table 1ab). The final steps ("sp4") leading from "p2" to "p3" in Figs.4,5,6 do not lead to any additional significant formation or growth of precipitates and can therefore be omitted. Nevertheless the calculated size distribution functions for "p2" and "p3" (Fig.7) used to evaluate the results in Figs.4,5,6 differ by an additional precipitation peak (C) as shown in Fig.7. The steps in Fig.7 show the calculation results for the 5 rate equations used in combination with a Fokker-Planck equation (continuous lines). The size distribution function for "p1" shows one precipitation peak (A) being characteristic for the $(1200°C)$ steps, while "p2" shows an additional one for the $1000°C$ anneal in "sp3" and "p3" a third one (C) for the $950°C$ step in "sp4".

The cooling rate in crystal growth is an important parameter for the amount of precipitation observed. This is demonstrated by reducing the cooling rate ("co2" instead of "co1" (Table 1ab)) leading from "p3" to "p4" in Figs.4,5,6. Enhanced precipitate formation and growth in the CMOS-type cycle is observed (compare "p4" to "p3" in Figs.4,5,6). From the calculated size-distribution functions plotted in Fig.8, it can be seen that precipitates formed during cooling in crystal growth are generated predominantly in the temperature range from 1000°C to 700°C. The high temperature cycle "sp1" was intended to dissolve these precipitates and make the results after the CMOS-cycle less sensitive to thermal conditions in crystal growth. The effectiveness of "sp1" can be improved using a steeper temperature ramp and inserting the wafers into the furnace at $1000°C$ instead of $850°C$ ("sp5" in Table 1ab). This allows less of the preexisting precipitates ("co1" in Fig.9) to grow on during the ramp up to $1200°C$ (dashed and dotted line in Fig.9) and leads to retardation of precipitation after the CMOS-type cycle ("p5" compared to "p3" in Figs.4,5,6).

4 Summary and conclusion

A general concept for systematically deriving coupled kinetic diffusion-precipitation equations has been proposed. Our recently developed computer model for oxygen precipitation is found to be in good agreement with a number of experimental results including CMOS-type anneals. It has been applied for investigating oxygen precipitation in order to help optimizing a CMOS-type annealing cycle. Temperature ramps and cooling in crystal growth are found to have a significant influence on the number and size of the precipitates after the CMOS-type cycle.

Acknowledgement - This work has been supported by the Fonds zur Förderung der wissenschaftlichen Forschung, project no. P7495-PHY.

References

[1] E.Guerrero, H.Pötzl, R.Tielert, M.Grasserbauer, G.Stingeder, J. Electrochem. Soc., Vol.129 (1982) 1826-1831.

[2] F.S.Ham, J.Phys.Chem.Solids, Vol.6 (1958)335-351.

[3] S. Messoloras, R.C.Newman and J.H.Tucker, Semicond.Sci.Technol. 2,(1987)14.

[4] J.I.Frenkel : "Kinetic Theory of Liquids", Dover, New York (1955).

[5] G.A. Hawkins and J.P.Lavine, J.Appl.Phys. **65**,3644 (1989).

[6] M.Schrems,T.Brabec,M.Budil,H.Pötzl,E.Guerrero,D.Huber, Materials Science and Engineering, B4 (1989)393-399.

[7] M.Schrems, P.Pongratz, M.Budil, H.Pötzl, J.Hage, E.Guerrero, D.Huber, Semiconductor Silicon 1990, (1990)144-155.

[8] M.Schrems, P.Pongratz, M.Budil, H.Pötzl, J.Hage, E.Guerrero, D.Huber, Proceedings of the ESSDERC'90, (1990)201-204.

[9] M.Orlowski, Proc. IEDM'90, (1990)729-732.

[10] C.W. Gardiner,"Handbook of Stochastic Methods " in "Springer Series in Synergetics" (1985).

[11] D.Turnbull and J.C.Fisher, J.Chem.Phys. **17**,71 (1949).

[12] J. Vanhellemont and C. Claeys, J.Appl.Phys. **62**,3960 (1987).

[13] K.Nishioka, Phys.Rev. A16(1977)2143.

[14] W.Jüngling, P.Pichler, S.Selberherr, E.Guerrero, H.Pötzl, IEEE J.Solid State Circuits Vol.SC-20 (1985)76-87.

[15] G.J.L. Ouwerling,F.van Rijs,B.F.P.Jansen,W.Crans NASCODE VI,Dublin, Boole Press (1989)78.

[16] W.Huber,M.Pagani,J.Electrochem.Soc.,Vol.137,(1990)3210-3213.

[17] R. Swaroop, N.Kim, W.Lin, M.Bullis, L.Shive, A.Rice, E.Castell, M.Christ, Solid State Technology/March (1987) 85-88.

[18] M.Schrems, P.Pongratz, M.Budil, H.Pötzl, J.Hage, E.Guerrero, D.Huber, Proc. of the Int.Conf. on Science and Technol. of Defect Control in Semiconductors, Yokohama, (1989).

[19] W.A.Craven, Semiconductor Silicon 1981, (1981)254-271.

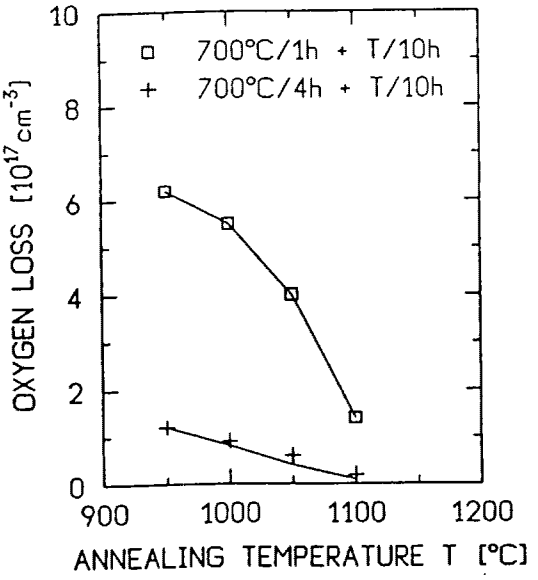

Figure 1: Reduction in the interstitial oxygen concentration as a function of the second annealing temperature in a double-step thermal process. Experimental results (squares and crosses)[17] and simulations (full lines) are shown.

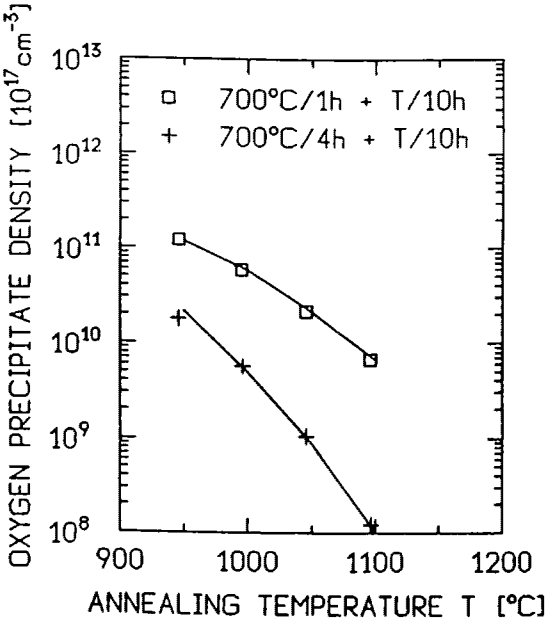

Figure 2: Concentration of oxygen precipitates as a function of the second annealing temperature in a double-step thermal process. Experimental results (squares and crosses)[17] and simulations (full lines) are shown.

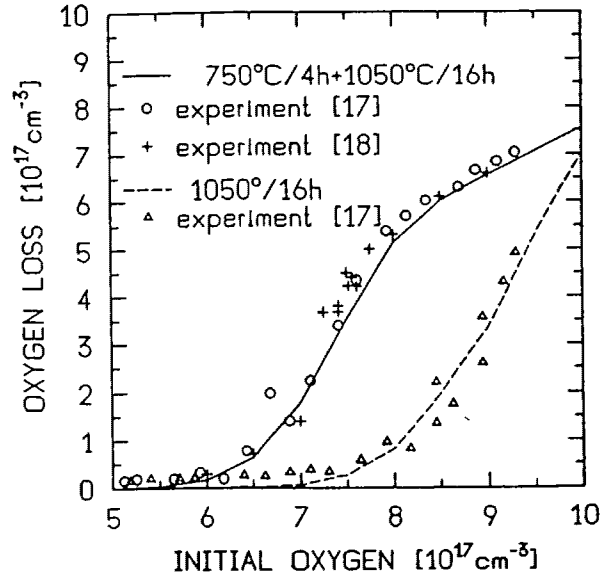

Figure 3: Oxygen loss vs. initial oxygen concentration for a double-step and a single-step anneal. The full and the dashed lines are simulations.

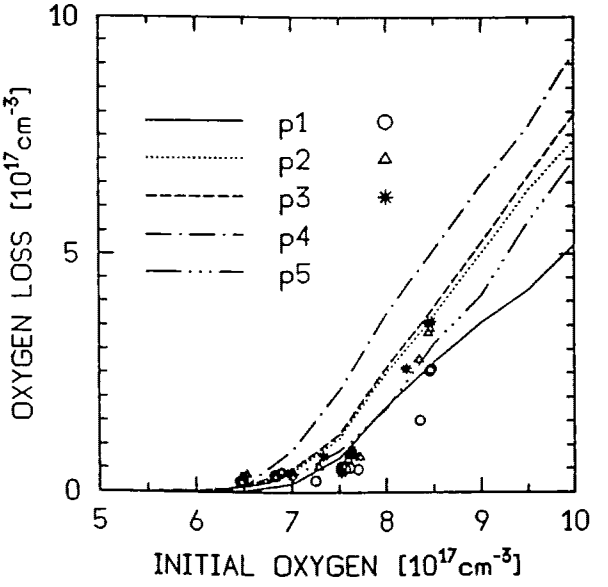

Figure 4: Oxygen loss vs. initial oxygen concentration calculated for 5 different CMOS-type thermal anneals specified in Tables 1ab. Circles, triangles and stars are experimental results for p1,p2, and p3 from Tables 1ab.

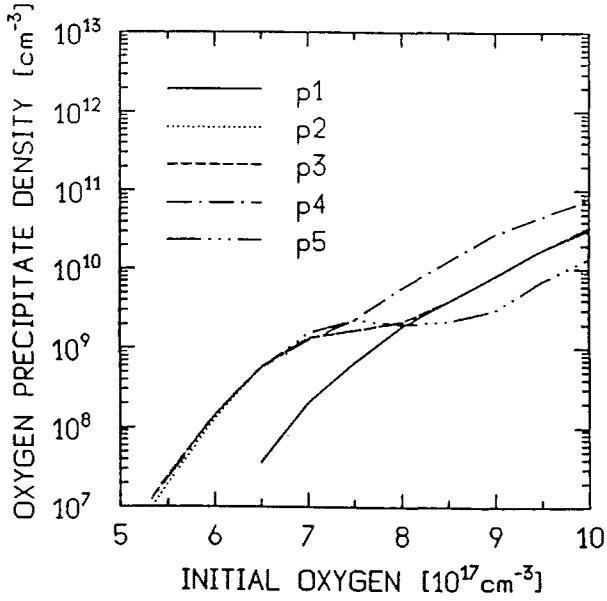

Figure 5: Concentration of oxygen precipitates vs. initial oxygen concentration calculated for 5 different CMOS-type thermal anneals specified in Tables 1ab.

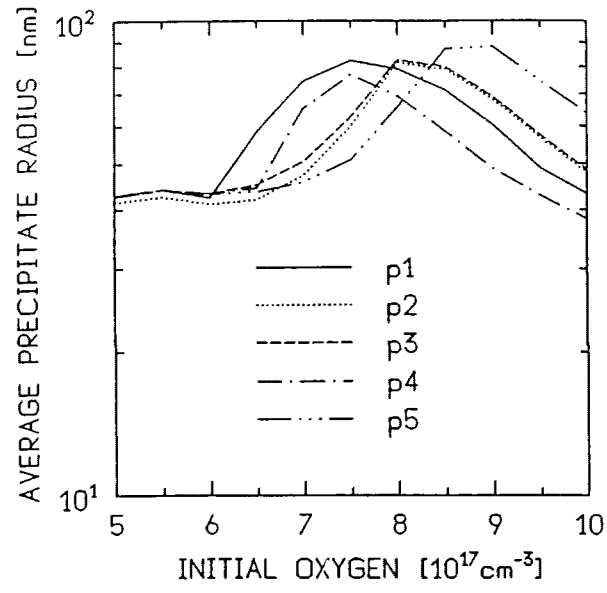

Figure 6: Average oxygen precipitate radius vs. initial oxygen concentration calculated for 5 different CMOS-type thermal anneals shown in Tables 1ab.

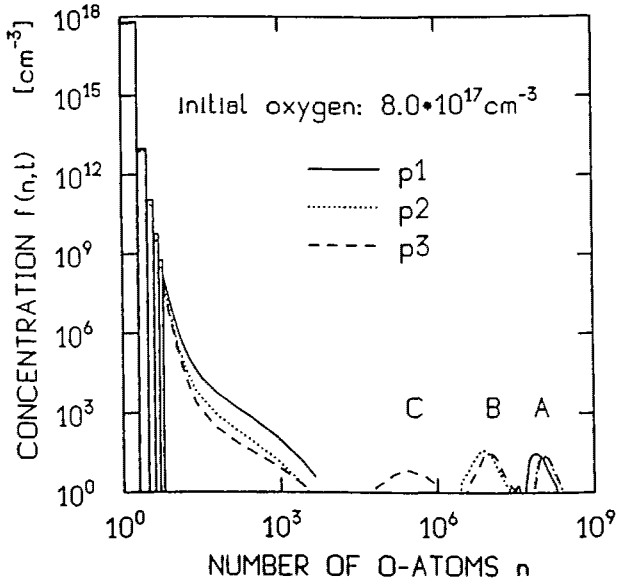

Figure 7: Concentration of oxygen precipitates vs. number of oxygen atoms in a precipitate (size-distribution function) calculated after p1,p2 and p3 shown in Tables 1ab. 5 rate equations (steps) in combination with a Fokker-Planck equation are used.

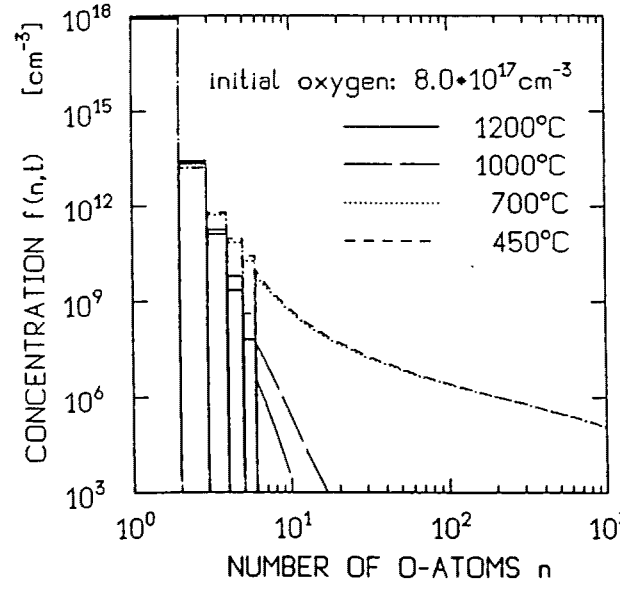

Figure 8: Calculated size-distribution functions shown at 4 succeeding temperatures during cooling in crystal growth.

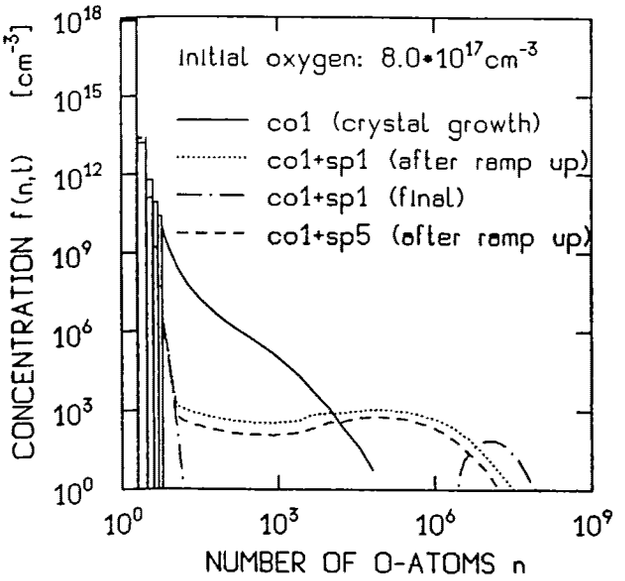

Figure 9: Calculated size-distribution function after cooling in crystal growth (full line), after ramp up (dotted line) and ramp down in subprocess sp1 (Table1b), and for comparison after ramp up in subprocess sp5.

CMOS-type cycles	
process=	sum of elements
p1=	co1+sp1+sp2
p2=	co1+sp1+sp2+sp3
p3=	co1+sp1+sp2+sp3+sp4
p4=	co2+sp1+sp2+sp3+sp4
p5=	co1+sp5+sp2+sp3+sp4

Table 1a

Elements of the CMOS-type cycles		
step	temperature	time
co1 (cooling 1)	1400°C →450°C	10 h
co2 (cooling 2)	1400°C →450°C	20 h
sp1 (subprocess 1)	850°C →1200°C	70 min
(precipitate	+ 1200°C	120 min
dissolution)	+ 1200°C → 850°C	70 min
sp2 (subprocess 2)	850°C → 950°C	20 min
(Oxidation)	+ 950°C	60 min
	+ 950°C →1100°C	30 min
	+ 1100°C →1200°C	50 min
(Well drive in)	+ 1200°C	300 min
	+ 1200°C → 850°C	175 min
sp3 (subprocess 3)		
(Nitridation)	800°C	200 min
	+ 800°C →1000°C	40 min
(Oxidation)	+ 1000°C	780 min
	+ 1000°C → 850°C	75 min
sp4 (subprocess 4)		
	800°C	60 min
	+ 800°C → 950°C	30 min
	+ 950°C	300 min
	+ 950°C → 850°C	50 min
sp5 (subprocess 5)	1000°C →1200°C	20 min
(precipitate	+ 1200°C	120 min
dissolution)	+ 1200°C → 850°C	70 min

Table 1b